Influence of mixing time on a reversal tolerant anode measured ex situ for a PEMFC

Homan, S. J.T.; Aylar, K.; Jurjevic, A.; Scolari, M.; Urakawa, A.; Taheri, P.

DOI
10.1016/j.ijhydene.2024.01.236

Publication date
2024

Document Version
Final published version

Published in
International Journal of Hydrogen Energy

International Journal of Hydrogen Energy 59 (2024) 1166–1173

Contents lists available at ScienceDirect

International Journal of Hydrogen Energy

journal homepage: www.elsevier.com/locate/he

Influence of mixing time on a reversal tolerant anode measured *ex situ* for a PEMFC

S.J.T. Homan [a,b,*], K. Aylar [a], A. Jurjevic [a], M. Scolari [a], A. Urakawa [b], P. Taheri [c]

[a] Cellcentric GmbH & Co. KG, Neue Str. 95, Kirchheim unter Teck, 73230, Germany
[b] Catalysis Engineering, Department of Chemical Engineering, Delft University of Technology, Van der Maasweg 9, Delft, 2629 HZ, The Netherlands
[c] Department of Materials Science and Engineering, Faculty of Mechanical, Maritime, and Materials Engineering, Delft University of Technology, Mekelweg 2, Delft, 2628 CD, The Netherlands

ARTICLE INFO

Keywords:
PEMFC
Reversal tolerant anode (RTA)
Catalyst layer processing
Rotating disc electrode (RDE)
OER catalyst

ABSTRACT

When no hydrogen can reach the Pt catalyst in the anode for the hydrogen oxidation reaction (HOR) of an operating proton exchange membrane fuel cell (PEMFC), the anode potential increases and causes the cell potential to be reversed compared to normal operation conditions. During this reversal, the oxygen evolution reaction (OER) and carbon oxidation reaction (COR) will occur at the anode, where the COR has devastating consequences for the electrode. Introducing an OER catalyst limits the COR to occur, which makes a reversal tolerant anode (RTA). In this research, RTAs are differentiated by applying different ball milling times during catalyst layer processing, forming big and small OER (IrO_x/TiO_x) and HOR (Pt/C) catalyst particles. The two different particle sizes were electrochemically tested using a rotating disc electrode (RDE). Both catalyst sizes show a decrease in OER activity (mA cm^{-2}) accompanied by loss of the ionomer in a self-developed accelerated stress test (AST). The small particle RTAs show higher OER activity as a result of increased surface area. However, during a chronopotentiometry measurement, which mimics a fuel cell reversal, the small particle coatings show a worse reversal tolerance. This phenomenon can be attributed to the increased difficulty in removing oxygen bubbles.

1. Introduction

The transport sector is responsible for 24% of the total CO_2 emission worldwide, making it one of the main contributors to climate change due to the combustion of fossil fuels [1]. The hydrogen economy is a school of thought, where fossil fuel combustion will be replaced while being CO_2 neutral and still meeting the global energy demand. In the hydrogen economy, hydrogen would be used as an energy carrier, which can be made by electrolysis with electricity from renewable energy sources [2]. This means that applications should be ready to convert hydrogen into the desired energy form. The fuel cell is such a device that can convert hydrogen along with oxygen to electricity and water. The PEMFC is currently the most suitable and used fuel cell for automotive applications due to its high power density, low weight, rapid start-up and low operating temperature [3].

A PEMFC stack is made up of electrochemical cells, which are known as a Membrane Electrode Assembly (MEA). In the MEA, the cathode and anode electrodes are separated by a proton exchange membrane. At the anode side the hydrogen oxidation reaction (HOR, E = 0.0 V vs RHE) takes place and the oxygen reduction reaction (ORR, E = 1.23 V vs RHE) at the cathode. Both reactions are generally catalyzed by platinum (Pt), which is deposited on a carbon support that allows electrical conduction and provides the porous structure [4]. Furthermore, a perfluorosulfonic acid (PFSA) ionomer is applied in the catalyst layer and allows proton transport between the catalyst particles and the membrane and functions as a binder [5,6]. Because the key electrochemical reactions occur at the electrodes, the performance of a PEMFC stack is directly dependent on the composition and structure of the catalyst layers. Therefore, degradation at the catalyst layer will directly result in a decrease in the performance of the PEMFC stack. To become a future success, durability is of crucial importance. Different organizations (e.g. US Department of Energy) have set 5000 h (8000 h in the long term) for automotive applications as the time where the PEMFC should still have 90% of its Begin of Life (BoL) performance [7]. Therefore, tackling the degradation phenomena that occur in the catalyst layer is a must for the future of the PEMFC.

* Corresponding author at: Catalysis Engineering, Department of Chemical Engineering, Delft University of Technology, Van der Maasweg 9, Delft, 2629 HZ, The Netherlands.
E-mail address: s.j.t.homan@tudelft.nl (S.J.T. Homan).

https://doi.org/10.1016/j.ijhydene.2024.01.236
Received 13 November 2023; Received in revised form 18 January 2024; Accepted 20 January 2024
Available online 14 February 2024

One of the degradation phenomena is carbon corrosion. It causes a decrease in thickness, which can be correlated with a collapse of the porous structure [8,9]. Furthermore, carbon corrosion can also cause detachment of the catalyst layer from the other components of the MEA, leading to an increase of resistance [10]. Additionally, the carbon gains more hydrophilic oxygen-containing groups, which alternate water management in the catalyst layer [11]. Finally, Pt nanoparticles can grow in size with carbon corrosion, leading to loss of electrochemical surface area (ECSA) and hence loss of performance [10–13]. At the anode, carbon corrosion occurs when hydrogen cannot reach the platinum catalyst (fuel starvation) [14]. Insufficient hydrogen delivery to the catalyst can be the result of a malfunction or blockage of the hydrogen in pores filled with liquid water or ice and will be more severe under rapid loading change or start-up conditions [15]. When there is no hydrogen for the HOR at the anode to deliver the required current and protons for the cathode's ORR, the potential of the anode will rise. The potential in the anode becomes higher than in the cathode, leading to a negative total cell potential ($V_{total} = V_{cathode} - V_{anode}$) (see Fig. 1) [14]. This is opposite to the potentials during normal operating conditions, and therefore the fuel starvation phenomenon is also known as fuel cell reversal. At higher potentials in the anode, other sources in its environment will be used for the oxidation reaction to deliver the required protons and electrons to the cathode. Water in the anode environment can be used for the oxygen evolution reaction (OER, E = 1.23 V vs RHE) and carbon and water for the carbon oxidation reaction (COR, E = 0.21 V vs RHE). The COR needs to be prevented because this is the reaction responsible for carbon corrosion. The COR also occurs at operating cell voltages at the cathode (0.6–0.8 V). However, due to the limiting kinetics, the COR starts to play a critical role in degradation at 1.1 V in the PEMFC catalyst layer with an increased reaction rate with increasing potential [16,17]. During fuel cell reversal, the cell can irreversibly lose its functionality within several minutes due to carbon corrosion at the anode.

To tackle this problem, system control mitigation strategies or material mitigation strategies can be applied. The former leads to a more fragile and expensive operating system, and due to its response time it still leaves the system open to damage from carbon corrosion [14]. Therefore, a material mitigation would be the preferred one. First, changes to the carbon support can be applied, to make the catalyst layer less prone to carbon corrosion [18,19]. Secondly, an OER catalyst can be introduced to the anode, which induces a preference for the OER over the COR, rendering this approach a reverse tolerant anode (RTA). The goal of the OER catalyst is to keep the potential low enough during fuel cell reversal to prevent the COR from dominating and destroying the anode. However, at some point, the potential starts to rise despite the presence of the OER catalyst. The time necessary to reach a certain cutoff potential is called the voltage reversal time (VRT) and the longer VRT is obviously desired (see Fig. 1).

To keep the potential as low as possible during fuel cell reversal, it is important to have the OER catalyst with the highest activity, which are generally alloys and/or oxides with ruthenium (Ru) and iridium (Ir) [20]. Of the two materials mentioned above, Ir is known to be the most stable in the harsh acidic conditions of the PEMFC [21,22]. Oakton et al. (2017) pointed out that titanium oxide (TiO_x) as a support for iridium oxide (IrO_x) can help to improve OER performance in acidic conditions while reducing costs [23]. In addition, different strategies can be applied to increase the VRT. For example, the VRT increases linearly with the amount of IrO_x applied to the anode [12,24,25]. Zhou et al. (2021) improved the VRT by applying different anode designs based on the uneven distribution of chemicals and potentials present [26]. Furthermore, Chen et al. (2021) found that decreasing thickness and increasing ionomer content of the catalyst layer increased the VRT [27]. Another way to improve resistance to fuel cell reversal is to deposit IrO_x as nanoparticles on the carbon support, which was found to improve activity, as well as VRT [28]. Using a carbon with increased functional oxygen groups, which acts as anchor points for IrO_x nanoparticles during deposition, increased the dispersion of OER nanoparticles and hence the activity and VRT [29].

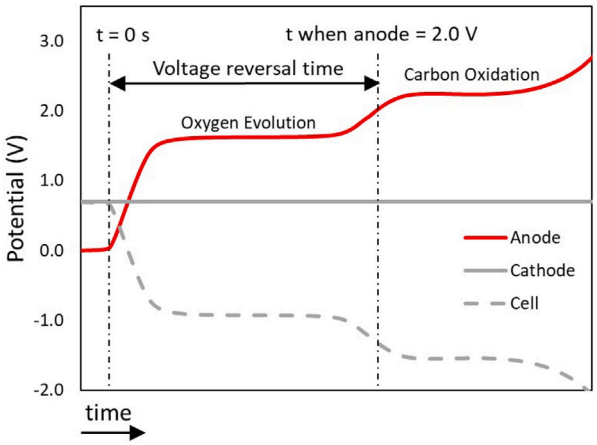

Fig. 1. The potentials during a fuel cell reversal, where the fuel starvation starts at $t = 0$ and the cut-off potential has been set at 2.0 V to determine the voltage reversal time (VRT) for the anode.

Most literature recognize the strong influence of the anode design on the reversal tolerance performance, nevertheless uncontrolled homogenization with ultrasonication is often encountered for the RTA [12,25–27,30–33]. At the cathode, the importance of ink homogenization and its effects on the catalyst layer structure and electrochemical performance are more recognized [34–40]. Therefore, in this research, the effect of controlled homogenization of the RTA ink was examined. During processing, a difference was made by applying different ball milling times to the ink (ionomer/HOR-catalyst/OER-catalyst/alcohol/water mixture), resulting in a controlled adjustment of the particle size distribution. The different particle sizes (μm scale) were electrochemically tested in an rotating disc electrode (RDE), to understand how the fundamental electrochemistry will be affected.

When measuring the whole MEA *in situ*, it is difficult to pinpoint the exact phenomena that occur due to its multi-component characteristic. On the contrary, the RDE can be used for electrochemical testing of the catalyst layer only, it is relatively fast, requires only a small amount of materials and is less complex than an MEA testing setup [41]. However, *ex situ* electrochemical testing of the OER is known to be troublesome, which can be devoted to the formation of oxygen bubbles at the RDE tip [42,43]. These oxygen bubbles are difficult to be removed and can give unreliable results due to blockage of space, which increases the difficulty of the reactant to reach the catalyst [44]. From a different perspective, this sensitivity of the RDE to oxygen bubble formation can be used to understand the effect of oxygen bubbles on different RTA designs. Therefore, an accelerated stress test (AST) has been developed and applied to understand how the activity and stability of the RTA develop over time at reversal potentials, with the objective of minimizing the effect of oxygen bubble formation. Degradation could be understood with material characterization techniques. Finally, to mimic fuel starvation in a RDE, chronopotentiometry protocols were applied to understand the effect of the different processed catalyst layers on the VRT.

2. Materials & methods

2.1. Ink mixing & coating

A schematic representation of the ink mixing and coating procedure is shown in Fig. 2. Platinum on carbon particles (Pt/C), iridium oxide supported on titanium oxide (IrO_x/TiO_x) and PFSA ionomer (equivalent weight < 900 g/mol) were placed in a beaker. Two different inks

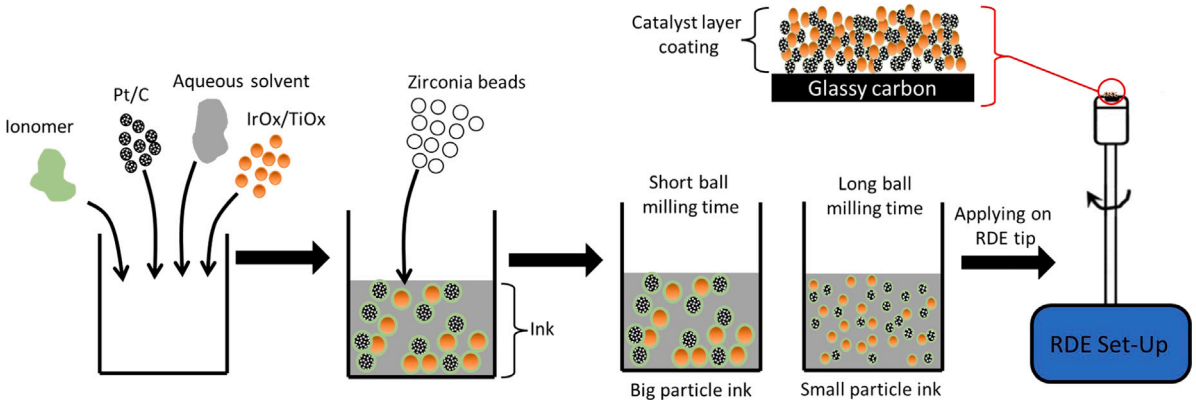

Fig. 2. A schematic overview of the processing method used.

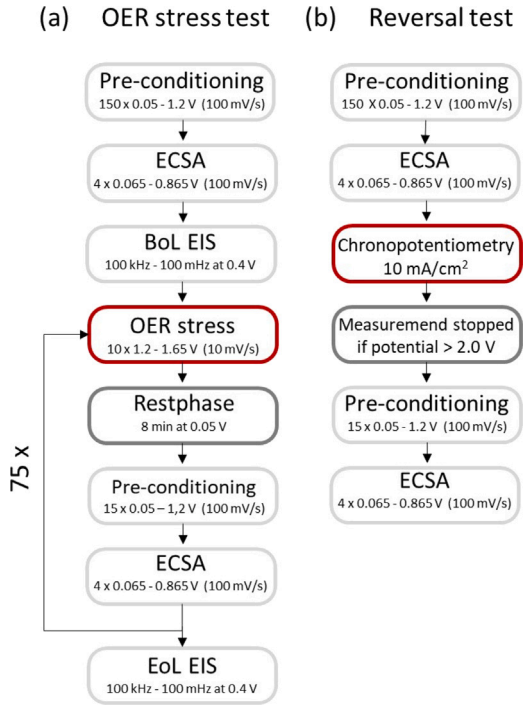

Fig. 3. The two electrochemical protocols that were developed and applied with 1600 RPM except for the pre-conditioning (0 RPM).

were made, differentiated by their ionomer to carbon weight ratios (I/C) of 0.8 and 1.0. Additionally, zirconia beads were applied for ball milling. During ball milling, the particle size distribution was followed by laser diffraction. Samples were taken after 45 and 240 min of ball milling, which were labeled as big particle and small particle ink, respectively. All RTA inks were spin-coated on a glassy carbon RDE tip. The RTAs were rotated at 300 RPM under ambient conditions until completely dried. The amount of ink applied was calculated, so that the weight of both Pt and Ir in the catalyst layer coating was equal to 50 μg cm^{-2}. The homogeneity and quality of the coated catalyst layer on the glassy carbon was observed with a Keyence laser microscope. Furthermore, the laser microscope was used to evaluate the surface roughness of the catalyst layer coatings on the micrometer scale. To have a reproducible and well-dispersed coating, the glassy carbon surface was well polished with alumina slurry (0.05 μm) before each coating procedure. After polishing, the working electrode was placed in an ultrasonic bath for 3 min.

2.2. Electrochemical tests

The coated RDE tip was placed in a 0.5 M H_2SO_4 electrolyte equipped with a H_2 reference electrode and a Pt working electrode. This was followed by pre-conditioning and an electrochemical surface area (ECSA) measurement, which was executed to remove surface impurities and activate the Pt catalyst surface [45]. Furthermore, Pt ECSA measurements were used as an additional control of the coating procedure and check for a shift in the H_2 reference electrode. The two protocols executed in this research can be described in Fig. 3. In the OER stress test, 75 cycles with 10 sweeps between 1.20 and 1.65 V were applied to induce OER stress. The pre-conditioning and ECSA measurements were performed to follow Pt degradation over time. Begin of Life (BoL) and End of Life (EoL) electrical impedance spectroscopy (EIS) were added in the electrochemical protocol of the OER stress test. The EIS results were fitted with the Transmission Line Model of a porous electrode, which provided information on the electrical and proton resistance of the RTA coating (see Supplemental Information Figs. S1 & S2). Furthermore, elemental surface analysis by XPS and SEM/EDS was performed on a small-particle BoL and EoL RTA. For this analysis, the catalyst layer coating needed to be transferred from the RDE tip. A few drops of 1-propanol were applied to the RDE tip to dissolve the RTA. This catalyst-containing solvent was deposited on an indium film followed by evaporation of the solvent. The BoL sample was coated on the RDE tip followed by the pre-conditioning and an ECSA measurement, before transferring and depositing it on indium. This was done so that the electrolyte contact and transfer procedure could not influence the differences between the EoL and BoL samples for material characterization. Finally, to mimic real fuel cell reversal in a RDE setup, chronopotentiometric measurements (at 10 mA cm^{-2}) with a cutoff potential of 2.0 V were performed.

3. Results and discussion

In Fig. 4 the particle size distribution as a function of the mixing time is shown. The volume-based diameter D90 (in μm) represents the value of which 90% of the particles are smaller than this value [46,47]. Therefore, it is an useful parameter to obtain the particle size distribution of the ink during the process. Fig. 4a shows a decreasing particle size distribution over time for the RTA inks analyzed in this research. It shows that no difference could be found between the two different I/C ratios applied. Additionally, inks were made with OER and HOR catalyst only, to understand the effect of ball milling time on the OER and HOR catalysts separately. These results are shown in Fig. 4b, where the initial particle size distribution of the OER particles is much broader than the HOR particles. However, the particle size distribution of the OER particles decreased strongly with an increasing mixing time and approached the D90 value of the HOR particles.

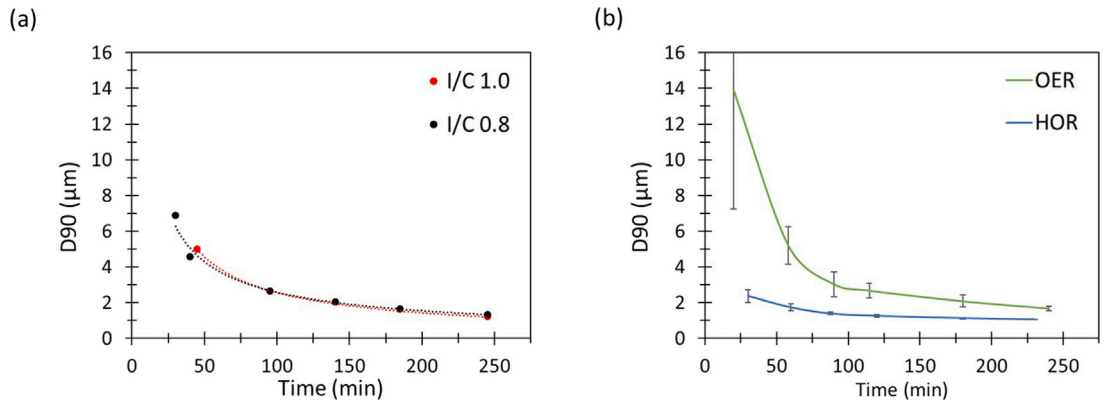

Fig. 4. The particle size distribution (D90) versus the ball milling time (a) shows the PSD of the RTA inks made in this research (b) averages of inks made of OER (IrOx/TiOx) catalyst only and inks made with HOR (Pt/C) catalyst only.

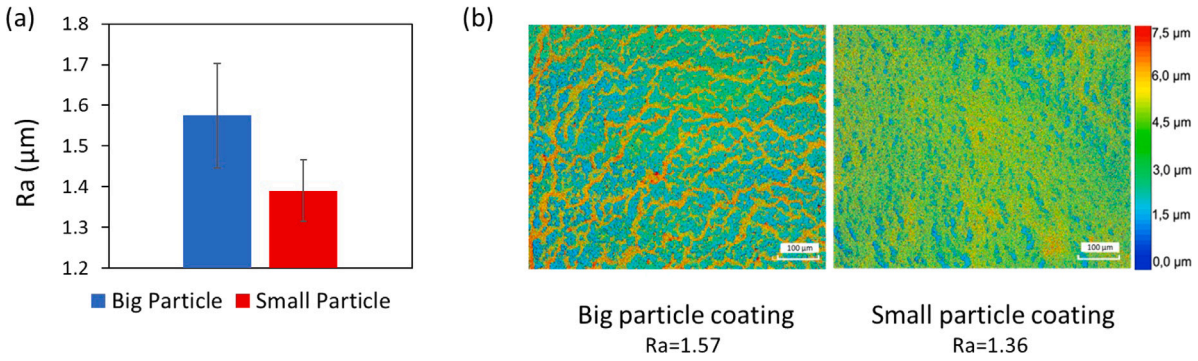

Fig. 5. Surface roughness (Ra) of coated RDE tips where (a) shows the difference between big particles and small particles and (b) a surface image of the big and small particle coating with the belonging roughness value (Ra) of that image.

The roughness of the big particle RTA coating (taken after 45 min mixing) and small particle RTA coating (taken after 240 min mixing) can be found in Fig. 5. The surface roughness of the big particle coatings was found to be higher than for the small particles. Furthermore, the big particle coatings show a larger standard deviation concerning the Ra values. The higher roughness and its larger standard deviation can be explained by the increased particle size distribution during the ink mixing. A broader particle size distribution in the ink causes a wider range of particle sizes in the catalyst layer coating, and hence increased roughness and standard deviation. There could not be a clear difference found between the surface roughness (Ra) of the inks with different I/C ratios, which is in line with the similar particle size distributions of the two inks. Neither a significant difference between the two I/C's could be observed by any other (electrochemical) measurements executed in this research. Therefore, inks with I/C = 0.8 and 1.0 were considered to be one for the remainder of this study.

To evaluate the OER activity, the voltage was swept 10 times back and forth between 1.20 and 1.65 V. As can be seen in Fig. 6, maximum activity decreased during these 10 sweeps. However, in the next cycle after the rest-phase, pre-conditioning and ECSA, the OER activity completely regenerated. The rest-phase at 0.05 V while maintaining rotation helped regenerate OER activity. This could be explained by the removal of the oxygen bubbles during the rest, which was observed to be physically removed from the coating surface and finally the complete RDE tip (see Supplemental Video). Furthermore, Pt is available in the catalyst layer, which can reduce the oxygen bubbles in the micropores through the ORR during the pre-conditioning and ECSA tests. Applying this cycle 75 times, the stability of OER activity over time was monitored while minimizing the effect of oxygen bubble formation (see Fig. 7). All the activities measured in the AST were reproducible. This means that the effect of the oxygen bubble formation

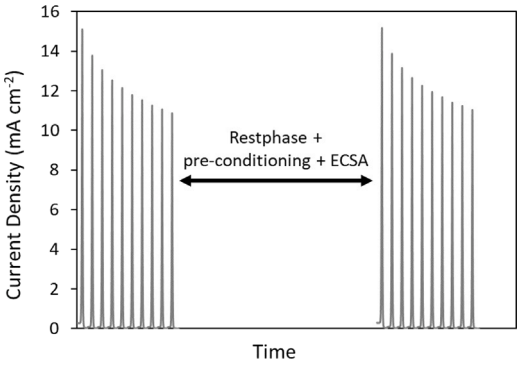

Fig. 6. The regeneration of the OER activity during the OER stress test (10 × 1.2 - 1.65 V with 10 mV s^{-1}), when a rest-phase is applied in between. The relative small activity of the pre-conditioning and ECSA is left out (between −5 mA cm^{-2} and 1 mA cm^{-2}).

on the OER activity occurs to the same extent. In other words, the RDE can be used to understand the effect of oxygen bubbles on the RTA. Within a cycle, the second sweep was found to have a smaller standard deviation than the first sweep. This could probably be due to the first sweep, which acts as a conditioning sweep for the OER catalyst. Because of this, the development of OER activity in the AST of the 2nd and 10th sweep, are shown in Fig. 7. The small particle RTAs show a higher OER activity during the AST compared to the big particle coatings. This can be attributed to the increased electrochemical surface area of the relatively smaller IrO_x/TiO_x particles. As shown in Fig. 4b, during the mixing process from 45 min to 240 min, the particle size distribution of the OER particles decreased approximately a five-fold.

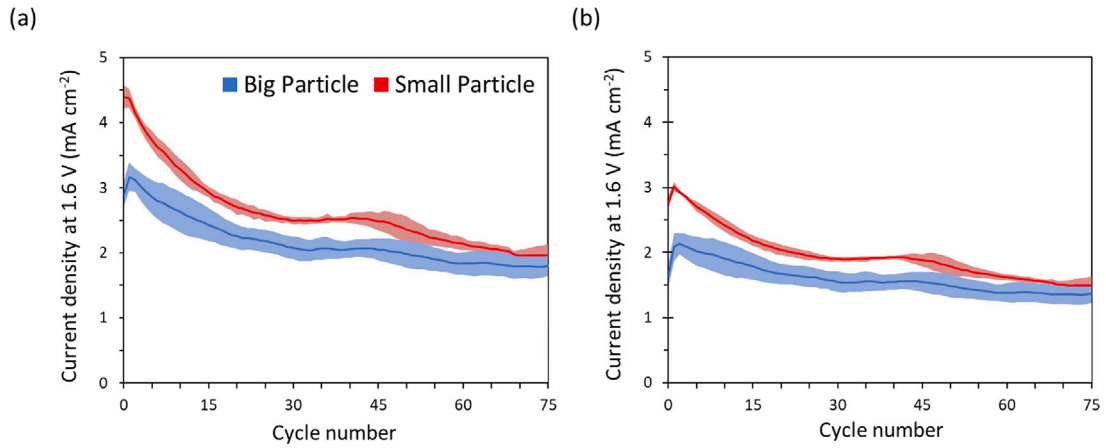

Fig. 7. The activity over time of the big (blue) and small particles (red), where the shaded colors indicate the standard deviation of the measurements and (a) belongs to the 2nd sweep within each cycle and (b) the 10th. (For interpretation of the references to color in this figure legend, the reader is referred to the web version of this article.)

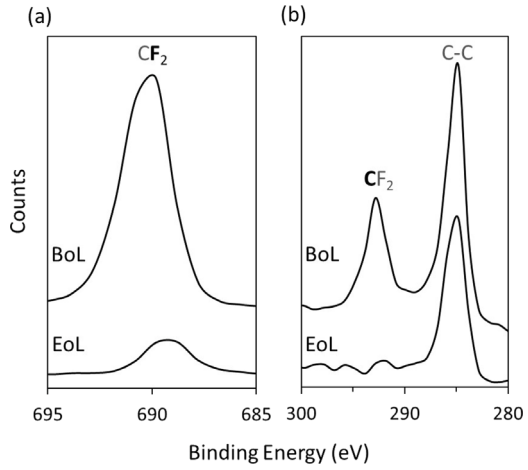

Fig. 8. XPS results, where (a) shows the fluoride region in the spectra and (b) carbon.

Therefore, increasing the mixing time, decreased the OER particle size, which increases the OER activity as a result of the increased surface area of the OER catalyst. Furthermore, the big particle RTAs have a lower activity and larger standard deviation, which corresponds to the larger standard deviation of particle sizes found in the ink and surface roughness of the coatings. Additionally, the results show that the activity decreases faster within a cycle at the beginning of the AST compared to the end of the AST. The activity of the small particle RTA decreases with 37% within the first cycle compared to 19% in the last cycle. This is explained by the increased oxygen production at a higher current density, since the moles of oxygen produced increases with the amount of electrons produced. Therefore, if more oxygen is produced at the beginning of a cycle, it will block more reactant at the end of a cycle. At the end of the AST, the RTA was degraded and hence the activity decreased. All measurements showed a decrease of OER activity during the AST. The Tafel slope was found to be similar between two RTA particle sizes and remained almost unchanged during the AST with an average of 54 ± 3 mV dec^{-1}. This also includes the averages within a cycle (see Supplemental Information Fig. S3 & Table S1). This is an indication that, during the AST, the OER kinetics remained most likely unchanged and that the loss of activity has other origins. If the oxidation state of IrO_x has changed and causes a difference in kinetics, it should be indicated by the Tafel slope [48].

In Fig. 8, the results of the XPS are shown. It shows that during the AST, the carbon peak at 285 eV has decreased slightly in intensity, whose position is an indicator for the carbon support material in Pt/C [49]. However, the carbon peak around 293 eV indicates carbon in CF_2 [50,51]. The intensity of this peak has been reduced completely compared to that of the carbon support peak at 285 eV. This trend can also be seen in the fluoride region, where the peak at 689 eV has decreased, which is an indicator of F in CF_2 [52]. This loss of fluoride was also confirmed by SEM/EDS, where the fluoride content decreased relatively for all materials present (see Supplemental Information Fig. S4 & Table S2). Electrical impedance spectroscopy (EIS) showed that both electron resistance and proton conductivity decreased (see Table 1). It should be noted that the absolute EIS values of the different measurements could not be compared directly with each other due to the extreme sensitivity of the EIS and the set-up limitations. Regardless of the large differences between the initial resistances found by EIS, no difference was found in the OER activity and Pt ECSA measurements (see Supplementary Information Table S3). Therefore, it can be concluded that the contact resistances did not influence the electrochemical measurements. Furthermore, during an AST the complete set-up was untouched, meaning that comparing the change from BoL to EoL is valid.

Table 1
Electrical impedance spectroscopy of a porous electrode fitted with the Transmission Line Model, where $\Delta R = R_{EoL}\text{-}R_{BoL}$.

	ΔR_{ele} (Ω)	ΔR_{ion} (Ω)
Small particles	−0.09 ± 0.04	1.90 ± 0.24
Big particles	−0.23 ± 0.21	1.94 ± 0.92

The decrease in fluoride, the decrease in carbon that is bound to the fluoride and the increase in proton resistance are all indications that the ionomer layer has been degraded. If there is loss of ionomer, then an increase of proton resistance is a direct result of that. In addition, if ionomer is lost, it means more Pt/C contact points due to agglomeration. This will decrease the electrical resistance. However, because of the high conductivity of carbon, this effect is thought to be much smaller than the increase in ionic resistance [10]. If the ionomer is responsible for the decrease in activity, it should also have been observed in pristine activity of the two different inks processed (I/C = 0.8 and I/C = 1.0). However, contrary to an MEA, in RDE there is an excess of protons present in the electrolyte. Because of this, the catalyst layer does not require the ionomer as a proton source for its electrochemical reactions. To observe a change in ionic conductivity by EIS in a RDE set-up, there should be a substantial difference in ionomer content. Singh et al. (2015) showed that a difference could be obtained between ionic conductivity of catalyst layers with no ionomer, low ionomer content and a high ionomer content, which had 5 times the amount of the ionomer content [53]. Besides, the ionomer in the

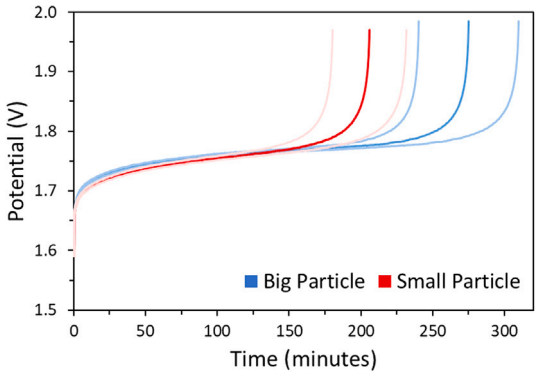

Fig. 9. Chronopotentiometry measurement to replicate fuel cell reversal on big and small particles executed at 10 mA cm^{-2}, where the shaded colors indicate the standard deviation of the measurements. (For interpretation of the references to color in this figure legend, the reader is referred to the web version of this article.)

RDE would still be necessary as a binder of the catalyst coating to the glassy carbon [54,55]. Therefore, it is suggested that the degradation of the ionomer in this AST is so severe that the whole catalyst layer's structure has changed and/or catalyst have been lost. In addition, multiple studies have indicated that IrO_x catalyst loss occurs due to dissolution in an RDE set-up, causing a loss of activity [31,56,57]. The loss of ionomer might induce IrO_x dissolution or the other way around. However, to the best of our knowledge, degradation of IrO_x as an OER catalyst in an RDE configuration is still a mechanism that is not clear at the moment [58]. But electrode structure and ionomer content should be taken into account.

The degradation of ionomer is believed to find its roots in radical formation. H_2O_2 can be formed in the ORR or OER, where the ORR is still occurring in the AST since there is Pt. Titanium oxide is a material that is known to form HO and HOO radicals out of the H_2O_2, which is also known as the Fenton reaction [59]. These radicals are then able to attack the PFSA ionomer, which destroys the functionality of the ionomer and creates HF and CO_2. Therefore, it would be suggested to avoid using titanium oxide in electrochemical systems that depend on the functionality of a PFSA ionomer [60,61]. In addition, loss of ionomer content and collapse of a structure are even more severe in a MEA compared to RDE as a result of an alternation of the water management and the dependence of gas transport of its reactants for the ORR and HOR [62]. Besides, the formed OH and HOO radicals in the catalyst layer could also potentially attack the membrane in a MEA, which in most cases is a PFSA ionomer.

The degradation of Pt was followed by ECSA over time and showed the same trend for all RTA's made and applied in the AST (see Supplemental Information Fig S5 & Table S3). This is due to the fact that there is always the same amount of voltage applied in all ASTs in this research. This means it is highly likely that the same amount of carbon corrosion takes place for all tests, regardless of how well the OER catalysts perform. The goal of the OER catalyst is to keep the potential low during fuel starvation to prevent further increase in potential and total destruction of the catalyst layer.

Therefore, to mimic fuel cell reversal, chronopotentiometry measurements were applied to the catalyst layers shown in Fig. 9. In the beginning, the potential of the big particle coating is slightly higher than that of the small particle coating. This is likely due to the higher activity of the small particle coating, which can keep a lower potential to produce a current density of 10 mA cm^{-2}. This initial difference between the two particle sizes increases when a higher current of 50 mA cm^{-2} was applied (see Supplementary Information Fig S6). However, the measurement was not reproducible as a result of the rapid growth of the oxygen bubbles at a higher current density. Additionally, 10 mA cm^{-2} was found as a reference point to test the stability of an OER catalyst in an RDE set-up [63–65].

It can be observed that regardless of the higher OER activity, the voltage reversal time is shorter for the smaller particles RTA than for the bigger particles at a chronopotentiometry measurement at 10 mA cm^{-2}. The potential rises sharply for the small particles (at 200 min) and big particles (275 min). This rapid increase in potential is less likely to arise from OER catalyst deactivation or dissolution, but rather originates from blockage by oxygen bubbles, which were physically observed to cover the whole RDE tip at the end of the measurement. It is suggested that small particle coatings have a decreased voltage reversal times as a result of the relatively more dense structure, which leaves less space for oxygen bubbles to escape compared to the more spacious big particle structure with larger pores [66]. In addition to the density difference of both structures, there is a possibility that the difference in surface roughness can also affect the ease of oxygen bubble release [67].

4. Conclusion

By applying different ball milling times during processing of the RTA, big and small particles catalyst coatings could be obtained. The big particle coatings were found to have a higher surface roughness on the μm scale. An accelerated stress test was developed to test the OER activity and stability of the RTA while trying to minimize the influence of oxygen bubbles. The electrode including smaller particles showed higher OER activity (mA cm^{-2}), due to the increase in the electrochemical surface area of the small particles. All electrode coatings of the two particle sizes showed a decrease in OER activity during the AST. This was accompanied by the loss of ionomer, which was confirmed by EIS and other material characterization techniques. The loss of ionomer content is suggested to have its origin in the Fenton reaction, which is promoted in the presence of titanium oxide. Even though the bigger catalyst particles has a lower OER activity, they showed an increased reversal tolerance performance. This could be devoted to the increased easiness of releasing oxygen bubbles in the bigger particles structure. Therefore, the rotating disc electrode was found to be an effective way of understanding how mixing time can influence OER activity and reversal tolerance. It highlights that optimizing and controlling the process is a necessity in order to improve the reversal tolerant anode.

Declaration of competing interest

The authors declare that they have no known competing financial interests or personal relationships that could have appeared to influence the work reported in this paper.

Appendix A. Supplementary data

Supplementary material related to this article can be found online at https://doi.org/10.1016/j.ijhydene.2024.01.236.

References

[1] Solaymani S. CO2 emissions patterns in 7 top carbon emitter economies: The case of transport sector. Energy 2019;168:989–1001. http://dx.doi.org/10.1016/j.energy.2018.11.145.

[2] Zornoza B, Casado C, Navajas A. Advances in hydrogen separation and purification with membrane technology. In: Gandía LM, Arzamendi G, Diéguez PM, editors. Renewable hydrogen technologies. Amsterdam: Elsevier; 2013, p. 245–68. http://dx.doi.org/10.1016/B978-0-444-56352-1.00011-8.

[3] Abderezzak B. Introduction to hydrogen technology. Elsevier; 2018, p. 1–51. http://dx.doi.org/10.1016/B978-1-78548-291-5.50001-9,

[4] Wendt H, Spinacé EV, Neto AO, Linardi M. Electrocatalysis and electrocatalysts for low temperature fuel cells: state of the art research and development. Quim Nova 2005;28:1066–75.

[5] Chen M, Zhao C, Sun F, Fan J, Li H, Wang H. Research progress of catalyst layer and interlayer interface structures in membrane electrode assembly (MEA) for proton exchange membrane fuel cell (PEMFC) system. eTransportation 2020;5. http://dx.doi.org/10.1016/j.etran.2020.100075.

[6] Suzuki A, Sen U, Hattori T, Miura R, Nagumo R, Tsuboi H, et al. Ionomer content in the catalyst layer of polymer electrolyte membrane fuel cell (PEMFC): Effects on diffusion and performance. Int J Hydrogen Energy 2011;36:2221–9. http://dx.doi.org/10.1016/j.ijhydene.2010.11.076, The Third Annual International Conference on Hydrogen Safety.

[7] Stropnik R, Mlakar N, Lotrič A, Sekavčnik M, Mori M. The influence of degradation effects in proton exchange membrane fuel cells on life cycle assessment modelling and environmental impact indicators. Int J Hydrogen Energy 2022;47(57):24223–41. http://dx.doi.org/10.1016/j.ijhydene.2022.04.011, Hydrogen Society.

[8] Randrianarizafy B, Schott P, Gerard M, Bultel Y. Modelling carbon corrosion during a PEMFC startup: Simulation of mitigation strategies. Energies 2020;13. http://dx.doi.org/10.3390/en13092338.

[9] Carter RN, Gu W, Brady B, Yu PT, Subramanian K, Gasteiger HA. Electrode degradation mechanisms studies by current distribution measurements. In: Handbook of fuel cells. John Wiley & Sons, Ltd; 2010, http://dx.doi.org/10.1002/9780470974001.f500055.

[10] Macauley N, Papadias DD, Fairweather J, Spernjak D, Langlois D, Ahluwalia R, et al. Carbon corrosion in PEM fuel cells and the development of accelerated stress tests. J Electrochem Soc 2018;165:F3148–60. http://dx.doi.org/10.1149/2.0061806jes.

[11] Zhang X, Yang Y, Guo L, Liu H. Effects of carbon corrosion on mass transfer losses in proton exchange membrane fuel cells. Int J Hydrogen Energy 2017;42:4699–705. http://dx.doi.org/10.1016/j.ijhydene.2016.08.223.

[12] Lim KH, Lee WH, Jeong Y, Kim H. Analysis of carbon corrosion in anode under fuel starvation using on-line mass spectrometry in polymer electrolyte membrane fuel cells. J Electrochem Soc 2017;164:F1580–6. http://dx.doi.org/10.1149/2.0731714jes.

[13] Taniguchi A, Akita T, Yasuda K, Miyazaki Y. Analysis of electrocatalyst degradation in PEMFC caused by cell reversal during fuel starvation. J Power Sources 2004;130:42–9. http://dx.doi.org/10.1016/j.jpowsour.2003.12.035.

[14] Qin C, Wang J, Yang D, Li B, Zhang C. Proton exchange membrane fuel cell reversal: A review. Catalysts 2016;6. http://dx.doi.org/10.3390/catal6120197.

[15] Hong BK, Mandal P, Oh JG, Litster S. On the impact of water activity on reversal tolerant fuel cell anode performance and durability. J Power Sources 2016;328:280–8. http://dx.doi.org/10.1016/j.jpowsour.2016.07.002.

[16] Maass S, Finsterwalder F, Frank G, Hartmann R, Merten C. Carbon support oxidation in PEM fuel cell cathodes. J Power Sources 2008;176(2):444–51. http://dx.doi.org/10.1016/j.jpowsour.2007.08.053.

[17] Roen LM, Paik CH, Jarvi TD. Electrocatalytic corrosion of carbon support in PEMFC cathodes. Electrochem Solid-State Lett 2003;7:A19. http://dx.doi.org/10.1149/1.1630412.

[18] Cherstiouk OV, Simonov AN, Moseva NS, Cherepanova SV, Simonov PA, Zaikovskii VI, et al. Microstructure effects on the electrochemical corrosion of carbon materials and carbon-supported Pt catalysts. Electrochim Acta 2010;55:8453–60. http://dx.doi.org/10.1016/j.electacta.2010.07.047.

[19] Forouzandeh F, Li X, Banham DW, Feng F, Ye S, Birss V. Understanding the corrosion resistance of meso- and micro-porous carbons for application in PEM fuel cells. J Electrochem Soc 2018;165:F3230–40. http://dx.doi.org/10.1149/2.0261806jes.

[20] Man IC, Su H-Y, Calle-Vallejo F, Hansen HA, Martínez JI, Inoglu NG, et al. Universality in oxygen evolution electrocatalysis on oxide surfaces. ChemCatChem 2011;3:1159–65. http://dx.doi.org/10.1002/cctc.201000397.

[21] Shi Z, Wang X, Ge J, Liu C, Xing W. Fundamental understanding of the acidic oxygen evolution reaction: mechanism study and state-of-the-art catalysts. Nanoscale 2020;12:13249–75. http://dx.doi.org/10.1039/D0NR02410D.

[22] Fabbri E, Habereder A, Waltar K, Kötz R, Schmidt TJ. Developments and perspectives of oxide-based catalysts for the oxygen evolution reaction. Catal Sci Technol 2014;4:3800–21. http://dx.doi.org/10.1039/C4CY00669K.

[23] Oakton E, Lebedev D, Povia M, Abbott DF, Fabbri E, Fedorov A, et al. IrO2-TiO2: A high-surface-area, active, and stable electrocatalyst for the oxygen evolution reaction. ACS Catal 2017;7:2346–52. http://dx.doi.org/10.1021/acscatal.6b03246.

[24] Mandal P, Hong BK, Oh JG, Litster S. Understanding the voltage reversal behavior of automotive fuel cells. J Power Sources 2018;397:397–404. http://dx.doi.org/10.1016/j.jpowsour.2018.06.083.

[25] Ahn C-Y, Kang SY, Choi HJ, Kim O-H, Sung Y-E, Cho Y-H. Effect of anode iridium oxide content on the electrochemical performance and resistance to cell reversal potential of polymer electrolyte membrane fuel cells. Int J Hydrogen Energy 2021;46:14713–23. http://dx.doi.org/10.1016/j.ijhydene.2021.01.199.

[26] Zhou X, Yang Y, Li B, Zhang C. Advanced reversal tolerant anode in proton exchange membrane fuel cells: Study on the attenuation mechanism during fuel starvation. ACS Appl Mater Interf 2021;13:2455–61. http://dx.doi.org/10.1021/acsami.0c16541.

[27] Chen W, Cai C, Li S, Tan J, Pan M. Thickness effects of anode catalyst layer on reversal tolerant performance in proton exchange membrane fuel cell. Int J Hydrogen Energy 2021;46:8749–57. http://dx.doi.org/10.1016/j.ijhydene.2020.12.041.

[28] Jang I, Hwang I, Tak Y. Attenuated degradation of a PEMFC cathode during fuel starvation by using carbon-supported IrO2. Electrochim Acta 2013;90:148–56. http://dx.doi.org/10.1016/j.electacta.2012.12.034.

[29] Kim H-E, Shin S, Lee H. Pt-IrOx catalysts immobilized on defective carbon for efficient reversal tolerant anode in proton exchange membrane fuel cells. J Catal 2021;395:404–11. http://dx.doi.org/10.1016/j.jcat.2021.01.028.

[30] Tovini MF, Hartig-Weiß A, Gasteiger HA, El-Sayed HA. The discrepancy in oxygen evolution reaction catalyst lifetime explained: RDE vs MEA - dynamicity within the catalyst layer matters. J Electrochem Soc 2021;168:014512. http://dx.doi.org/10.1149/1945-7111/abdcc9.

[31] Knöppel J, Möckl M, Escalera-López D, Stojanovski K, Bierling M, Böhm T, et al. On the limitations in assessing stability of oxygen evolution catalysts using aqueous model electrochemical cells. Nature Commun 2021;12. http://dx.doi.org/10.1038/s41467-021-22296-9.

[32] da Silva GC, Mayrhofer KJJ, Ticianelli EA, Cherevko S. Dissolution stability: The major challenge in the regenerative fuel cells bifunctional catalysis. J Electrochem Soc 2018;165(16):F1376. http://dx.doi.org/10.1149/2.1201816jes.

[33] Xu W, Scott K. The effects of ionomer content on PEM water electrolyser membrane electrode assembly performance. Int J Hydrogen Energy 2010;35(21):12029–37. http://dx.doi.org/10.1016/j.ijhydene.2010.08.055, VIII symposium of the Mexican Hydrogen Society.

[34] Li B, Liu Y, Guo Y, Yang D, Yang D, Ming P, et al. Controlling the microscopic morphology and permeability of catalyst layers in proton exchange membrane fuel cells by adjusting catalyst ink agglomerates. Int J Hydrogen Energy 2021;46(63):32215–25. http://dx.doi.org/10.1016/j.ijhydene.2021.06.216.

[35] Bapat S, Fricke S, Kohsakowski S, Goessling S, Peinecke V, Segets D. Tailoring of electrocatalyst inks for performance enhancement in proton exchange membrane fuel cells. ECS Trans 2020;97(7):651. http://dx.doi.org/10.1149/09707.0651ecst.

[36] Yang D, Guo Y, Tang H, Yang D, Ming P, Zhang C, et al. Effect of rheological properties of catalyst slurry on the structure of catalyst layer in PEMFC. Int J Hydrogen Energy 2022;47:8956–64. http://dx.doi.org/10.1016/j.ijhydene.2021.12.227.

[37] Kuroki H, Onishi K, Asami K, Yamaguchi T. Catalyst slurry preparation using a hydrodynamic cavitation dispersion method for polymer electrolyte fuel cells. Ind Eng Chem Res 2019;58(42):19545–50. http://dx.doi.org/10.1021/acs.iecr.9b02111.

[38] Du S, Li W, Wu H, Abel Chuang P-Y, Pan M, Sui P-C. Effects of ionomer and dispersion methods on rheological behavior of proton exchange membrane fuel cell catalyst layer ink. Int J Hydrogen Energy 2020;45(53):29430–41. http://dx.doi.org/10.1016/j.ijhydene.2020.07.241.

[39] Adamski M, Peressin N, Holdcroft S, Pollet BG. Does power ultrasound affect Nafion® dispersions? Ultrason Sonochem 2020;60:104758. http://dx.doi.org/10.1016/j.ultsonch.2019.104758.

[40] Wang M, Park JH, Kabir S, Neyerlin KC, Kariuki NN, Lv H, et al. Impact of catalyst ink dispersing methodology on fuel cell performance using in-situ X-ray scattering. ACS Appl Energy Mater 2019;2(9):6417–27. http://dx.doi.org/10.1021/acsaem.9b01037.

[41] Riese A, Banham D, Ye S, Sun X. Accelerated stress testing by rotating disk electrode for carbon corrosion in fuel cell catalyst supports. J Electrochem Soc 2015;162:F783–8. http://dx.doi.org/10.1149/2.0911507jes.

[42] van der Heijden O, Park S, Eggebeen JJ, Koper MT. Non-kinetic effects convolute activity and tafel analysis for the alkaline oxygen evolution reaction on NiFeOOH electrocatalysts. Angew Chem Int Edn 2022. http://dx.doi.org/10.1002/anie.202216477.

[43] Trogisch N, Koch M, Sawy ENE, El-Sayed HA. Microscopic bubble accumulation: The missing factor in evaluating oxygen evolution catalyst stability during accelerated stress tests. ACS Catal 2022;12:13715–24. http://dx.doi.org/10.1021/acscatal.2c03881.

[44] Hartig-Weiss A, Tovini MF, Gasteiger HA, El-Sayed HA. OER catalyst durability tests using the rotating disk electrode technique: The reason why this leads to erroneous conclusions. ACS Appl Energy Mater 2020;3:10323–7. http://dx.doi.org/10.1021/acsaem.0c01944.

[45] Martens S, Asen L, Ercolano G, Dionigi F, Zalitis C, Hawkins A, et al. A comparison of rotating disc electrode, floating electrode technique and membrane electrode assembly measurements for catalyst testing. J Power Sources 2018;392:274–84. http://dx.doi.org/10.1016/j.jpowsour.2018.04.084.

[46] Wang Y-H, Zhang Q-Q, Guo Y-Y, Xu F. Effect of flour particle size on the qualities of semi-dried noodles and fine dried noodles. J Food Process Preserv 2021;45(7):e15632. http://dx.doi.org/10.1111/jfpp.15632.

[47] Salazar J, Müller RH, Möschwitzer JP. Performance comparison of two novel combinative particle-size-reduction technologies. J Pharm Sci 2013;102(5):1636–49. http://dx.doi.org/10.1002/jps.23475.

[48] Siracusano S, Baglio V, Grigoriev S, Merlo L, Fateev V, Aricò A. The influence of iridium chemical oxidation state on the performance and durability of oxygen evolution catalysts in PEM electrolysis. J Power Sources 2017;366:105–14. http://dx.doi.org/10.1016/j.jpowsour.2017.09.020.

[49] Motin AM, Haunold T, Bukhtiyarov AV, Bera A, Rameshan C, Rupprechter G. Surface science approach to Pt/carbon model catalysts: XPS, STM and microreactor studies. Appl Surface Sci 2018;440:680–7. http://dx.doi.org/10.1016/j.apsusc.2018.01.148.

[50] Parry V, Berthomé G, Joud J-C, Lemaire O, Franco AA. XPS investigations of the proton exchange membrane fuel cell active layers aging: Characterization of the mitigating role of an anodic CO contamination on cathode degradation. J Power Sources 2011;196(5):2530–8. http://dx.doi.org/10.1016/j.jpowsour.2010.11.027.

[51] Zhu XL, Liu SB, Man BY, Xie CQ, Chen DP, Wang DQ, et al. Analysis by using X-ray photoelectron spectroscopy for polymethyl methacrylate and polytetrafluoroethylene etched by KrF excimer laser. Appl Surface Sci 2007;253:3122–6. http://dx.doi.org/10.1016/j.apsusc.2006.07.002.

[52] Moulder J, Chastain J. Handbook of x-ray photoelectron spectroscopy: a reference book of standard spectra for identification and interpretation of XPS data. Physical Electronics Division, Perkin-Elmer Corporation; 1992.

[53] Singh RK, Devivaraprasad R, Kar T, Chakraborty A, Neergat M. Electrochemical impedance spectroscopy of oxygen reduction reaction (ORR) in a rotating disk electrode configuration: Effect of ionomer content and carbon-support. J Electrochem Soc 2015;162:F489–98. http://dx.doi.org/10.1149/2.0141506jes.

[54] Shinozaki K, Morimoto Y, Pivovar BS, Kocha SS. Suppression of oxygen reduction reaction activity on Pt-based electrocatalysts from ionomer incorporation. J Power Sources 2016;325:745–51. http://dx.doi.org/10.1016/j.jpowsour.2016.06.062.

[55] Schmidt J, Gasteiger HA, Stab GD, Urban PM, Koib DM, Behm RJ. Characterization of high-surface-area electrocatalysts using a rotating disk electrode configuration. J Electrochem Soc 1998;145.

[56] Cherevko S, Reier T, Zeradjanin AR, Pawolek Z, Strasser P, Mayrhofer KJ. Stability of nanostructured iridium oxide electrocatalysts during oxygen evolution reaction in acidic environment. Electrochem Commun 2014;48:81–5. http://dx.doi.org/10.1016/j.elecom.2014.08.027.

[57] Cherevko S, Geiger S, Kasian O, Mingers A, Mayrhofer KJ. Oxygen evolution activity and stability of iridium in acidic media. Part 2. - Electrochemically grown hydrous iridium oxide. J Electroanal Soc 2016;774:102–10. http://dx.doi.org/10.1016/j.jelechem.2016.05.015.

[58] Diklić N, Beard A, Herranz J, Heinritz A, Cen T, Garbe S, et al. Breaking down the performance losses in O 2 -Evolution stability tests of IrO 2 -based electrocatalysts. J Electrochem Soc 2023;170:074503. http://dx.doi.org/10.1149/1945-7111/ace741.

[59] Tengvall P, Lundström I, Sjöqvist L, Elwing H, Bjursten LM. Titanium-hydrogen peroxide interaction: model studies of the influence of the inflammatory response on titanium implants. Biomaterials 1989;10(3):166–75. http://dx.doi.org/10.1016/0142-9612(89)90019-7.

[60] Xie M, Chu T, Wang T, Wan K, Yang D, Li B, et al. Preparation, performance and challenges of catalyst layer for proton exchange membrane fuel cell. Membranes 2021;11. http://dx.doi.org/10.3390/membranes11110879.

[61] Dreizler AM, Roduner E. Reaction kinetics of hydroxyl radicals with model compounds of fuel cell polymer membranes. Fuel Cells 2012;12(1):132–40. http://dx.doi.org/10.1002/fuce.201100157.

[62] Young AP, Stumper J, Knights S, Gyenge E. Ionomer degradation in polymer electrolyte membrane fuel cells. J Electrochem Soc 2010;157(3):B425. http://dx.doi.org/10.1149/1.3281899.

[63] Geiger S, Kasian O, Mingers AM, Nicley SS, Haenen K, Mayrhofer KJ, et al. Catalyst stability benchmarking for the oxygen evolution reaction: The importance of backing electrode material and dissolution in accelerated aging studies. ChemSusChem 2017;10:4140–3. http://dx.doi.org/10.1002/cssc.201701523.

[64] McCrory CC, Jung S, Peters JC, Jaramillo TF. Benchmarking heterogeneous electrocatalysts for the oxygen evolution reaction. J Am Chem Soc 2013;135:16977–87. http://dx.doi.org/10.1021/ja407115p.

[65] Spöri C, Kwan JTH, Bonakdarpour A, Wilkinson DP, Strasser P. Stabilitätsanforderungen von elektrokatalysatoren für die sauerstoffentwicklung: der weg zu einem grundlegenden verständnis und zur minimierung der katalysatordegradation. Angew Chem 2017;129:6088–117. http://dx.doi.org/10.1002/ange.201608601.

[66] Yong Y, Lou X, Li S, Yang C, Yin X. Direct simulation of the influence of the pore structure on the diffusion process in porous media. Comput Math Appl 2014;67(2):412–23. http://dx.doi.org/10.1016/j.camwa.2013.08.032, Mesoscopic Methods for Engineering and Science (Proceedings of ICMMES-2012, Taipei, Taiwan, 23–27 July 2012).

[67] Xiao Y, Zheng J, He Y, Wang L. Droplet and bubble wetting behaviors: The roles of surface wettability and roughness. Colloids Surf A 2022;653. http://dx.doi.org/10.1016/j.colsurfa.2022.130008.